Volume 7 | Number 5 | 7 March 2020

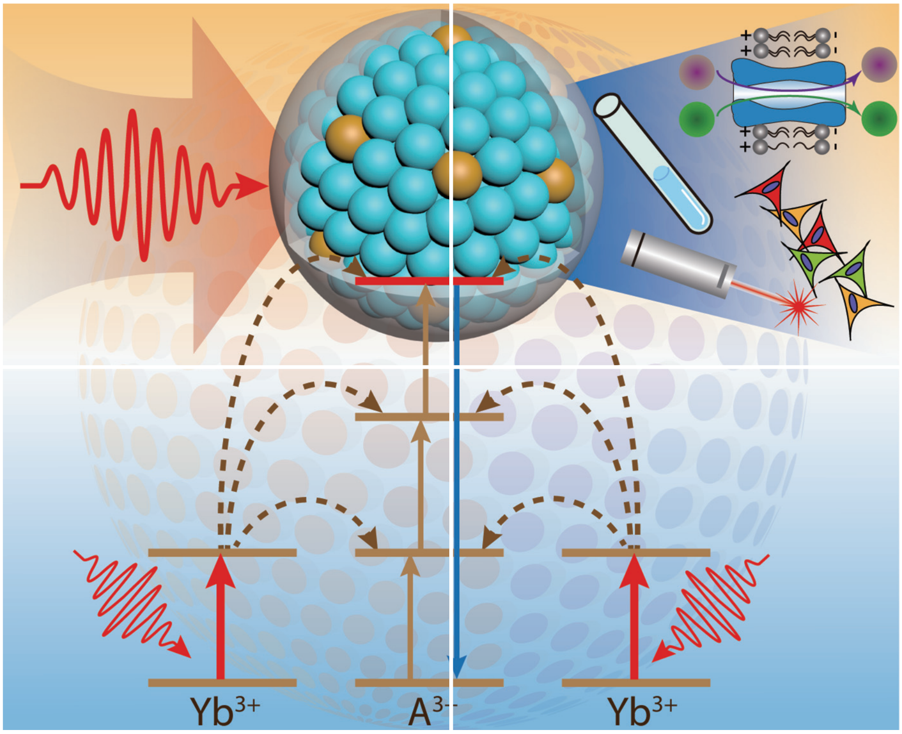

INORGANIC CHEMISTRY

FRONTIERS

CCS 中国化学会
CHINESE CHEMICAL SOCIETY

PEKING UNIVERSITY 1898

ROYAL SOCIETY OF CHEMISTRY

rsc.li/frontiers-inorganic

INORGANIC CHEMISTRY FRONTIERS

REVIEW

View Article Online
View Journal | View Issue

Cite this: *Inorg. Chem. Front.*, 2020, **7**, 1067

Recent advances in the synthesis and application of Yb-based fluoride upconversion nanoparticles

Bing Chen[a,b] and Feng Wang*[a,b]

Received 18th October 2019,
Accepted 6th December 2019

DOI: 10.1039/c9qi01358j

rsc.li/frontiers-inorganic

Lanthanide-doped upconversion nanoparticles are undergoing extensive investigations in many fields, particularly in biophotonics and photophysics. In an attempt to boost upconversion emission intensities, Yb-based fluoride crystals have been recently identified as more efficient alternatives to classical $NaYF_4$ crystals. Yb-Based fluoride crystals featuring a maximal occupancy of the host lattice by Yb^{3+} sensitizers facilitate the utilization of excitation light and promote energy transfer to upconverting activators, which contributes to a significant enhancement of upconversion luminescence. In this article, we present a survey of recent studies on chemical preparations of Yb-based fluoride nanoparticles with well-defined size and morphology. We show that these Yb-based upconversion nanoparticles are playing important roles in a few emerging applications such as optogenetics, biodetection and upconversion lasing.

1. Introduction

With advances in theoretical and experimental studies over the past few decades, the process of photon upconversion has attracted increasing attention in diverse fields ranging from biomedical science to information technology.[1–7] It is well accepted that rare earth fluorides (*e.g.*, $NaYF_4$) are the most suitable host materials for upconversion. The low phonon energy and high chemical stability of these materials give rise to a greatly reduced multiphonon relaxation rate and minimized non-radiative losses for lanthanide emitters (*i.e.*, Er^{3+}, Tm^{3+} and Ho^{3+}). In most cases, Yb^{3+} ions are co-doped into the hosts as sensitizers to increase the absorption cross-section in the near-infrared (NIR) at 980 nm.[8–14] Generally, the doping concentration of Yb^{3+} sensitizers is stringently kept at a low level to reduce harmful cross-relaxation and energy migration. For example, $NaYF_4$:Yb/Er (18/2 mol%) and $NaYF_4$:Yb/Tm (19/1 mol%) has been identified as the optimal composition in bulk crystals for producing green and blue upconversion emissions.[15] These classical formulas were also widely

---

[a] *Department of Materials Science and Engineering, City University of Hong Kong, 83 Tat Chee Avenue, Hong Kong SAR, China. E-mail: fwang24@cityu.edu.hk*
[b] *City University of Hong Kong Shenzhen Research Institute, Shenzhen 518057, China*

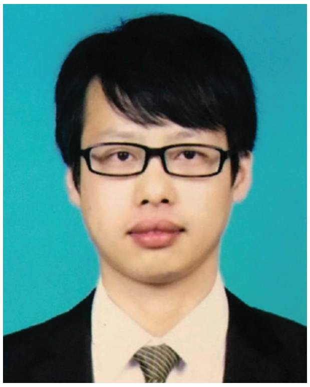

Bing Chen

Bing Chen was born in Zhejiang, China. He received his BE (2012) and PhD (2017) degrees in Materials Science and Engineering from Zhejiang University under the supervision of Prof. Xianping Fan. He is currently a postdoctoral fellow in Prof. Feng Wang's group at the City University of Hong Kong. His research interests focus on the development of luminescent micro/nanomaterials comprising lanthanide ions.

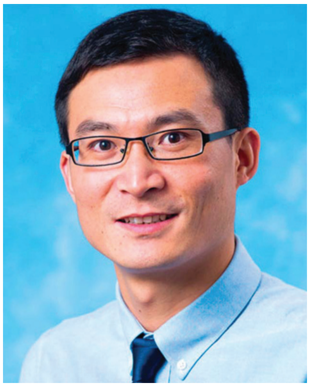

Feng Wang

Feng Wang is an Associate Professor at the City University of Hong Kong. He obtained his BE and PhD degrees in Materials Science and Engineering from Zhejiang University under the supervision of Prof. Minquan Wang and Prof. Xianping Fan. He completed his postdoctoral research work with Prof. Xiaogang Liu at the National University of Singapore and the Institute of Materials Research and Engineering in Singapore. His current research focuses on the synthesis, spectroscopic investigation, and application of micro/nanostructured luminescent materials.

employed in the construction of upconversion nanoparticles (UCNPs) over the past decade.[16–20]

The remarkable advantages of upconversion include a large anti-Stokes shift, sharp emission bandwidth and long excited-state lifetime.[21,22] However, widespread applications of UCNPs have encountered difficulties due to limited emission intensities. The relatively low content of Yb^{3+} sensitizers in conventional UCNPs typically results in a large transmission loss of incident light and thus ineffective excitation processes.[23] Some physical and chemical approaches such as excitation regulation and dye sensitization have been applied to improve the upconversion emission intensity.[24–27] However, these methods either suffer from a complex experimental setup or poor stability associated with organic components, which impose new constraints in practical applications.

Spectroscopic investigations on UCNPs have revealed that quenching processes associated with energy migration in Yb^{3+} ions can be largely minimized by leveraging the size and structure features of nanocrystalline hosts. Consequently, Yb-based hosts have been widely employed to construct UCNPs for maximizing the emission intensity in recent years.[28] Yb-Based UCNPs provide maximal concentrations of Yb^{3+} sensitizers in the host lattice, which elevates the absorption cross-section of the nanoparticles and promotes the utilization of excitation light. Given that the energy trapping by quenching centres is minimized, the Yb-based host lattice also offers accelerated energy transfer to activators due to a reduced ionic distance. As a result of the efficient excitation processes, Yb-based hosts could provide considerably enhanced multiphoton upconversion compared to the corresponding yttrium-based materials comprising a relatively low concentration of Yb^{3+} dopants.

In this review, we survey recent progress in the development of Yb-based fluoride UCNPs. We summarize various types of host materials being investigated and discuss protocols for the controlled synthesis of the nanoparticles. We also attempt to highlight emerging technological applications enabled by these Yb-based UCNPs.

2. Chemical synthesis

The crystalline structure of the host lattice determines the coordination environment of the dopant ions such as site symmetry and interionic distance. These parameters largely dictate intra-particle energy transfer and thus the photon upconversion processes. To date, a series of Yb-based UCNPs such as $LiYbF_4$, $BaYbF_5$, KYb_2F_7 and $NaYbF_4$ with distinct crystalline phases have been constructed and examined for upconversion (Fig. 1).[29–34] By using the as-synthesized nanoparticles as building blocks, a diversity of heterogeneous nanostructures have also been fabricated that provide added control over the properties and functionality of the UCNPs.

2.1. Controlled synthesis of homogeneous nanoparticles

The synthesis of Yb-based UCNPs is generally adapted from the protocols developed for the preparation of $NaYF_4$ or $NaGdF_4$ nanoparticles with minor modifications.[35] The most successful routes are the thermal decomposition of metal-tri-

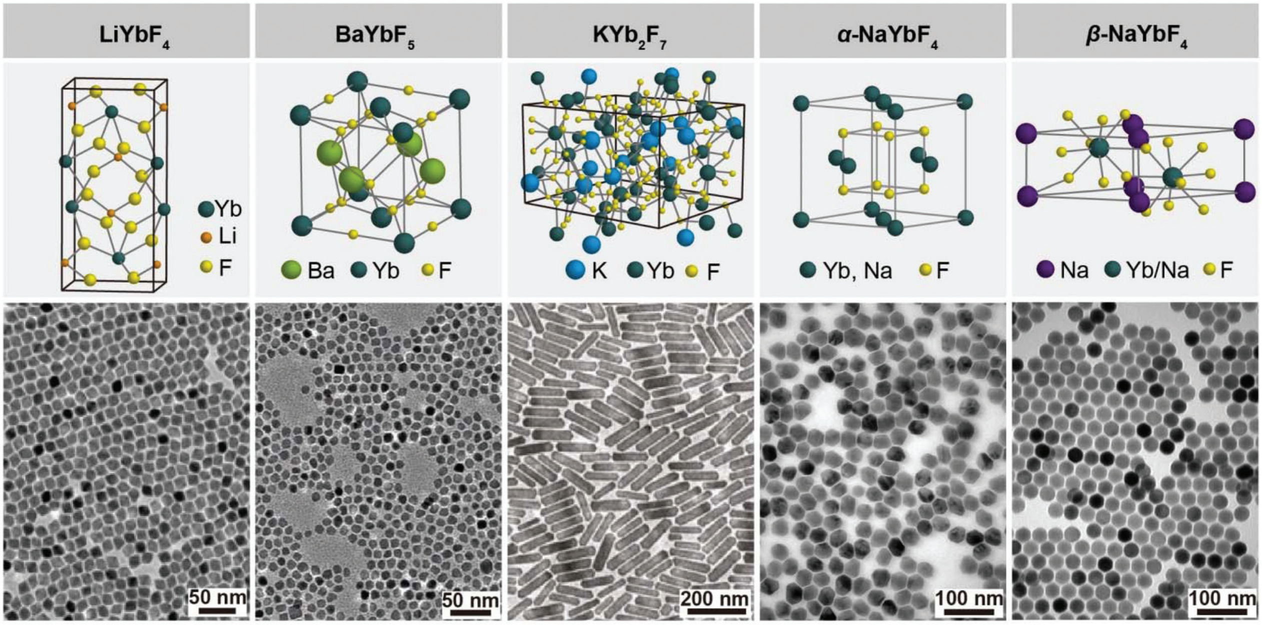

Fig. 1 An overview of common Yb-based fluoride hosts in the literature, which include $LiYbF_4$, $BaYbF_5$, KYb_2F_7, α-$NaYbF_4$ and β-$NaYbF_4$. Top panel: Crystalline structures of the fluoride hosts. Bottom panel: Typical TEM images of the corresponding nanoparticles. Reprinted with permission from ref. 29–31, 33 and 34. Copyright 2017 the Royal Society of Chemistry, 2012 WILEY-VCH Verlag GmbH & Co., 2014 Springer Nature, 2018 the Royal Society of Chemistry, and 2019 American Chemical Society, respectively.

fluoroacetates and precipitation of metal-oleate by fluoride in organic solvents.[36,37] By rational control over the synthetic parameters such as metal precursors, solvent composition, reaction time and temperature, uniform nanoparticles with tunable size can be readily prepared. For example, regular $LiYbF_4$ nanoparticles were previously synthesized by the coprecipitation reaction in a mixture solvent comprising trioctylamine (TOA) and oleic acid (OA),[34] while $BaYbF_5$ nanoparticles were synthesized in a sole solvent of OA.[31] The synthesis of KYb_2F_7 nanoparticles employed a mixed potassium precursor containing KOH and KF.[33] Cubic phase $NaYbF_4$ (α-$NaYbF_4$) nanoparticles can be obtained in a hot-injection technique using lanthanide trifluoroacetate precursors.[30]

Among various Yb-based fluoride host materials, hexagonal phase $NaYbF_4$ (β-$NaYbF_4$) draws the most attention. β-$NaYbF_4$ is isostructural with classical β-$NaYF_4$, which is beneficial for energy transfer upconversion processes.[38] However, β-$NaYbF_4$ tends to grow into relatively large crystals (>100 nm) under typical conditions for synthesizing other types of UCNPs. To this end, several specialized techniques have been developed to control the formation of β-$NaYbF_4$ nanoparticles, which can be summarised as dopant control, template control, precursor control, ligand control and temperature control (Fig. 2).

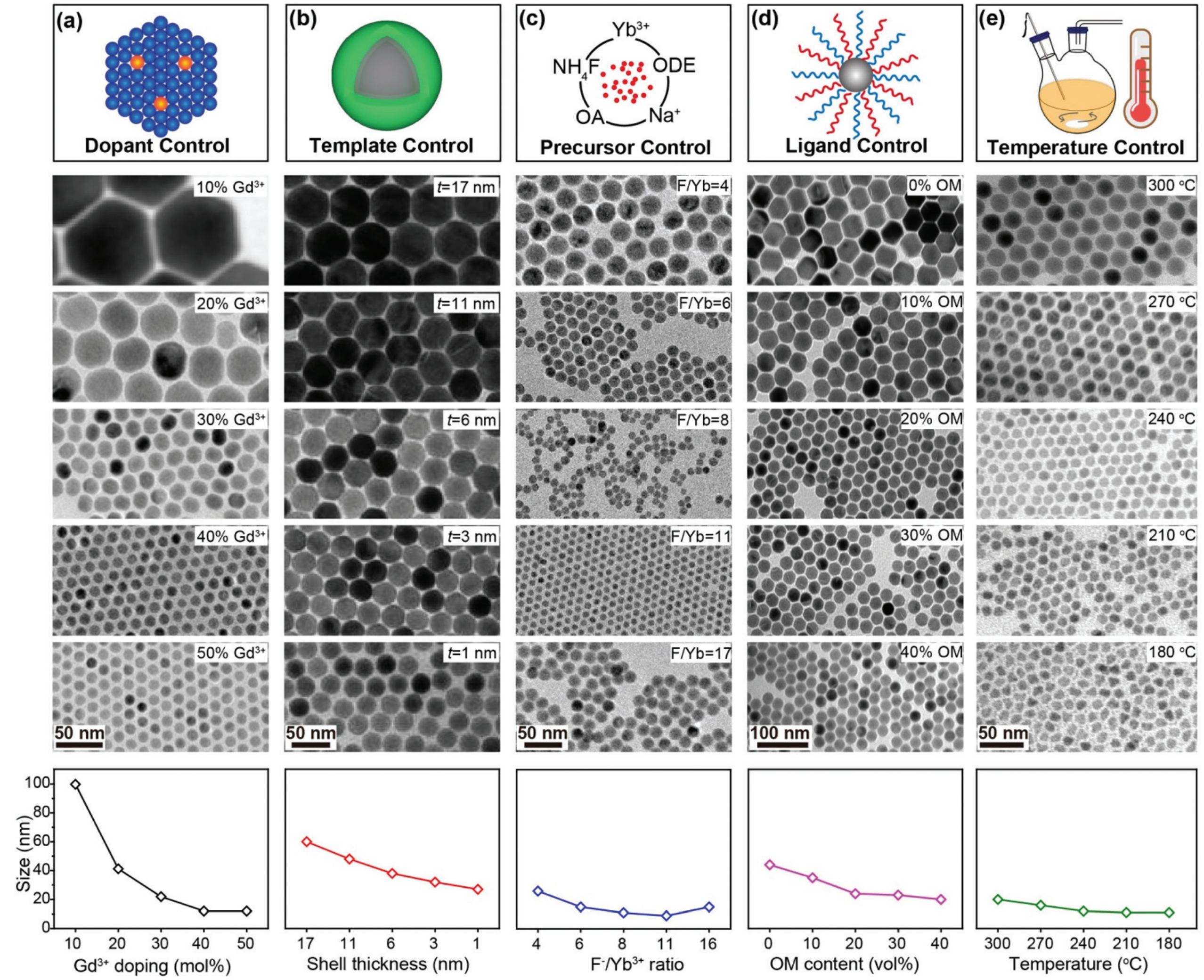

Fig. 2 The general synthetic strategies for preparing small β-$NaYbF_4$ nanoparticles with tunable size. Top panels: Illustrations of five representative strategies. Middle panels: Typical TEM images of β-$NaYbF_4$ nanoparticles with tunable size obtained by the corresponding strategies. Bottom panels: Size distributions showing the tunability of the corresponding strategies. (a) The dopant control strategy involving the incorporation of additional lanthanide ions (typically Gd^{3+}) into the host. Nanoparticle size is regulated by control of doping concentration. (b) The template control strategy involving the use of seed nanoparticles as the template (typically $NaYF_4$) for the direct epitaxial growth of β-$NaYbF_4$. The final size of the nanoparticles is determined by the seed size and the shell thickness (t). (c) The precursor control strategy regulating nanoparticle size by changing the F/Yb ratio in the starting materials. (d) The ligand control strategy for controlling nanoparticle formation by an elaborate selection of surfactant or chelating agents (*i.e.*, OM) in the synthesis. (e) The temperature control strategy for controlling nanoparticle size by regulating nucleation and crystal growth processes at different reaction temperatures. Reprinted with permission from ref. 28, 29, 40 and 45. Copyright 2014 American Chemical Society, 2016 Springer Nature, 2017 the Royal Society of Chemistry, and 2019 American Chemical Society, respectively.

Lanthanide impurity (*e.g.*, Gd^{3+}) doping was earlier reported as an effective solution for reducing the size of β-$NaYF_4$ UCNPs.[39] First-principles calculations revealed that the influence of lanthanide doping on nanocrystal size arises from the modification of surface charge density due to a large dipole polarizability of the substitutional dopants.[39] Following this guidance, Prasad and co-workers designed a Gd^{3+} doping approach to synthesize β-$NaYbF_4$:Tm^{3+} (0.5 mol%) UCNPs with tunable size (Fig. 2a).[40] They found that the substitution of Gd^{3+} (10 mol%) for Yb^{3+} yielded large β-$NaYbF_4$ nanoparticles with an average diameter of 100 nm. Gradually increasing the Gd^{3+} doping concentration from 20 to 50 mol% led to a continuous size decrease from 40 nm to 12 nm. Density functional theory (DFT) calculations confirmed that the Gd^{3+} dopants modulate the crystal growth by slowing down the diffusion of F^- ions to the nanocrystal surface due to increased surface charge repulsion.[39] Although the strategy of dopant control gives a convenient and wide control over the β-$NaYbF_4$ nanoparticle size (from 12 nm to 100 nm), the excessive introduction of Gd^{3+} impurities inevitably dilutes the β-$NaYbF_4$ lattice and thus compromises upconversion emissions.

To avoid the unnecessary inclusion of impurities, efforts have been made to grow β-$NaYbF_4$ nanoparticles on preformed β-$NaYF_4$ nanoparticles (Fig. 2b).[28] One distinct advantage of the seeded growth is that the nanoparticle size (or shell thickness) can be precisely controlled by adjusting the mass ratio of shell and core components.[41] In a representative example, our group succeeded in growing uniform β-$NaYbF_4$ layers with tunable thickness from 1 to 17 nm on 26 nm $NaYF_4$ nanoparticles by simply controlling the concentration of $NaYbF_4$ precursors.[29] However, the seeded growth typically involves tedious preparation steps for the deposition of multi-layered structures. Moreover, the range of nanoparticle sizes that can be accessed by this method is limited by the seed nanoparticles. The use of ultra-small seed nanoparticles in this type of synthesis may not be viable due to possible element diffusion across the core/shell interface.[42–44]

In an attempt to directly synthesize small β-$NaYbF_4$ UCNPs without the need of other rare earth elements, Huang and co-workers reported a precursor control route to synthesize small β-$NaYbF_4$ UCNPs by continuously changing the experimental variable of F^- to Yb^{3+} ratio (Fig. 2c).[45] They found that a stoichiometric ratio of F^- to Yb^{3+} (4 : 1) yielded uniform β-$NaYbF_4$ nanoparticles of 27 nm. As the ratio of F^- to Yb^{3+} increased from 6 : 1 to 11 : 1, the size of the resulting β-$NaYbF_4$ nanoparticles gradually decreased from 15 nm to 9 nm. However, a further increase in the F^-/Yb^{3+} ratio to 17 : 1 would somewhat reversely increase the nanoparticle size back to 15 nm. Although this precursor control method demonstrates an easy way to tune the size of β-$NaYbF_4$ nanoparticles, the range of size tunability is narrow and the underlying mechanism is not very clear.

Recently, our group demonstrated a quick and facile approach for preparing small β-$NaYbF_4$ nanoparticles by control of the ligand composition and reaction temperature (Fig. 2d and e).[29] Our approach involves a quick injection of metal-oleate precursors and ammonium fluoride (NH_4F) into a ternary solvent mixture of OA, 1-octadecene (ODE) and oleylamine (OM) at 310 °C. The introduction of OM ligands is identified to regulate phase transformation from intermediate α-$NaYbF_4$ to the final products of β-$NaYbF_4$ nanoparticles. Following this protocol, the size of β-$NaYbF_4$ nanoparticles could be accurately tuned from 44 nm to 15 nm along with a gradual increase of OM concentration (Fig. 2d). This OM-mediated synthesis was also demonstrated for the preparation of $LiYbF_4$ nanoparticles by Vetrone and co-workers,[46] who tuned the size of $LiYbF_4$ nanoparticles down to 5 nm by changing the ratio between the coordinating ligands of OA and OM.

We further noted that the existence of OM tremendously reduced the temperature needed for phase transformation from α-$NaYbF_4$ to β-$NaYbF_4$. Thus, along with a reduction in reaction temperature to 180 °C, the nanoparticle size was further tuned to as small as 7 nm (Fig. 2e).[29] Although these findings imply a flexible technique for low-temperature and large-scale synthesis of small-sized β-$NaYbF_4$ UCNPs, the low crystallinity degree of these nanoparticles prepared under low-temperature would inevitably compromise upconversion performance.

2.2. Synthesis and assembly of heterogeneous nanostructures

Yb-Based homogeneous UCNPs show limited utility due to their weak emission and incompatibility with most applications. Therefore, surface modification is typically applied to these UCNPs for enhancing the emission intensity and functionality. In addition, the UCNPs are often integrated with other types of nanomaterials to acquire new opportunities for upconversion modulation.

The large specific surface area of small UCNPs generally leads to severe surface-related quenching processes. Surface quenching is particularly significant in Yb-based UCNPs, because the excitation energy of the interior ions can be readily transferred to the surface by energy migration through the Yb sublattice.[47,48] In this regard, an inert and uniform protection shell is essential to isolate the upconversion core from surface quenching centres (Fig. 3a).[49]

The criteria for the selection of protection shell materials include high optical inertness and small lattice mismatch. A Y-based shell is commonly used in the protection of upconversion cores. For example, we previously prepared a series of β-$NaYF_4$@$NaYbF_4$@$NaYF_4$ core–shell–shell UCNPs using a layer-by-layer growth method.[28,49] Due to a large difference in atomic numbers between Yb ($Z = 70$) and Y ($Z = 39$), contrasts between the constituent layers of the core–shell–shell structure can be clearly seen under high-angle annular dark-field (HAADF) scanning TEM (Fig. 3b). Except for $NaYF_4$, $NaLuF_4$ shells are also frequently used for the epitaxial coating of $NaYbF_4$ cores. $NaLuF_4$ displaying a very close lattice parameter and similar growth behaviours to $NaYbF_4$ can form uniform and thick coating layers on $NaYbF_4$ UCNPs.[29] We recently examined the effect of $NaLuF_4$ shell thickness on the upconversion emission intensity of β-$NaYbF_4$:Er (2 mol%)@$NaLuF_4$

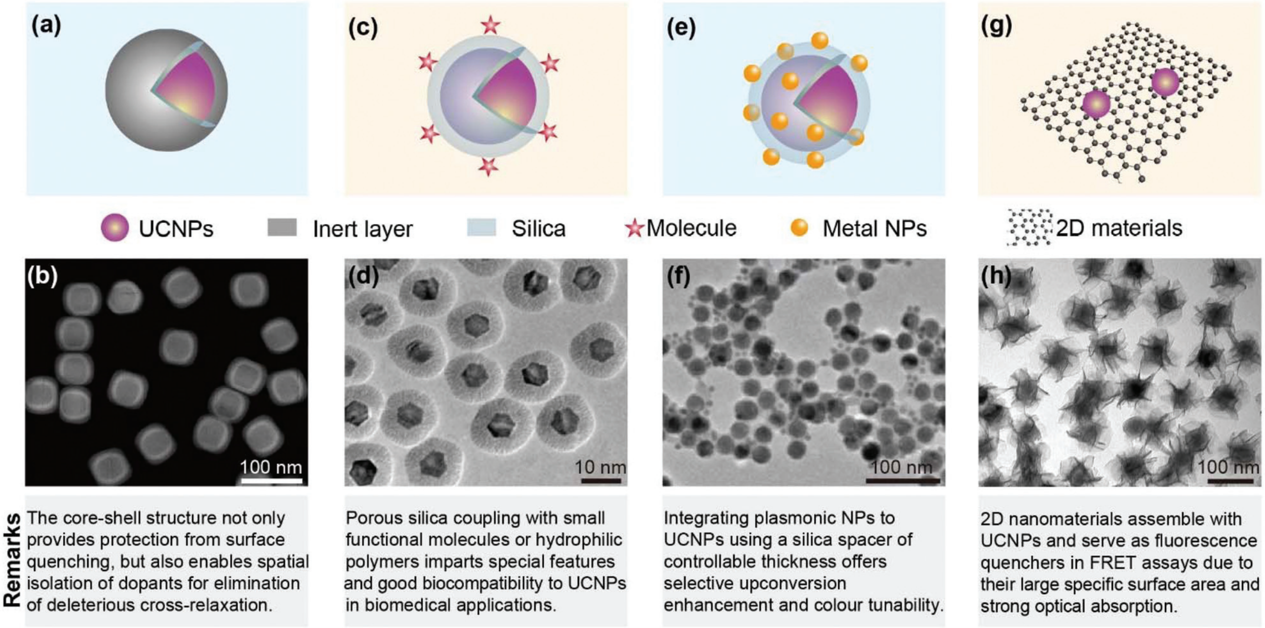

The core-shell structure not only provides protection from surface quenching, but also enables spatial isolation of dopants for elimination of deleterious cross-relaxation.

Porous silica coupling with small functional molecules or hydrophilic polymers imparts special features and good biocompatibility to UCNPs in biomedical applications.

Integrating plasmonic NPs to UCNPs using a silica spacer of controllable thickness offers selective upconversion enhancement and colour tunability.

2D nanomaterials assemble with UCNPs and serve as fluorescence quenchers in FRET assays due to their large specific surface area and strong optical absorption.

Fig. 3 Strategies of synthesizing and assembling heterogeneous nanostructures. (a) A core–shell structure isolates the dopant ions with the surroundings. (b) HAADF-STEM image of β-$NaYF_4$@$NaYbF_4$:Ho (1 mol%)@$NaYF_4$ core–shell–shell nanoparticles showing the contrasts between the constituent layers. (c) The design of $mSiO_2$ coating for coupling functional molecules to the UCNPs. (d) TEM image of typical β-$NaGdF_4$:Yb/Er/Ca@$NaYbF_4$:Ca@$NaNdF_4$:Gd/Ca @$mSiO_2$ nanoparticles. (e) The schematic of using silica shell as a spacer for coupling metal nanoparticles to the UCNPs. (f) TEM image of β-$NaYbF_4$:Tm (1 mol%)@SiO_2 (3.0 nm)@In nanocomposites. (g) The design of 2D layered nanomaterials for constructing FRET systems. (h) TEM image of MnO_2-modified α-$NaYbF_4$:Tm (1 mol%)@CaF_2 nanocomposites. Reprinted with permission from ref. 30, 49, 57 and 81. Copyright 2016 and 2018 American Chemical Society, 2019 WILEY-VCH Verlag GmbH & Co., and 2018 the Royal Society of Chemistry, respectively.

core–shell nanoparticles. The results showed that a thick shell is typically needed to provide an effective protection of the core nanoparticles against surface quenching. In our study, the maximum enhancement of core emission by over 700-fold was achieved at a shell thickness of 10 nm.[29]

The other feature of the core–shell design is that the shell layer can be incorporated with active lanthanide ions for tuning the upconversion luminescence. A typical example is doping Nd^{3+} sensitizers in the shell layer to expand the excitation spectrum. The high content of Yb^{3+} in the core ensures the effective capture of Nd^{3+} energy at the core/shell interface, leading to efficient upconversion processes by excitation at multiple wavelengths such as 798, 808 and 868 nm.[50] As an added benefit of the core/shell design, Nd^{3+} sensitizers and activators (*e.g.*, Er^{3+}, Tm^{3+} and Ho^{3+}) are separated in different layers and their direct interactions are thus avoided, which would otherwise cause significant quenching of excitation energy.[51,52]

To facilitate the technological applications of Yb-based UCNPs, a mesoporous silica ($mSiO_2$) coating was developed to impart hydrophilicity, biocompatibility and surface functionality (*e.g.*, –COOH, –NH_2, –SH) to the nanoparticles.[53] Moreover, $mSiO_2$ provides the possibilities of incorporating various molecules into the microchannels of silica shells by physical adsorption or chemical grafting (Fig. 3c). Based on the nanocomposites of UCNPs and $mSiO_2$, many NIR-triggered photodynamic therapy (PDT) agents were designed.[54–56] For example, Yang and co-workers constructed a multi-layered β-$NaGdF_4$:Yb/Er@ $NaYbF_4$@$NaNdF_4$@$mSiO_2$-PEG-RB nanocomposite for PDT (Fig. 3d).[57]

The UCNP@$mSiO_2$ design is versatile for loading various kinds of therapeutic agents. In addition to photosensitizers, chemotherapy drugs have also been successfully installed in the nanocomposites.[58,59] For example, an NIR light-triggered anticancer drug release system was developed by Shi and coworkers, who integrated $NaYF_4$:Yb/Tm@$NaYF_4$@$mSiO_2$, doxorubicin (Dox) and photo-responsive azobenzene (azo) molecules together in single nanohybrids.[60] The important advantages of the NIR-activated UCNP@$mSiO_2$ nanocomposites as the light transducer and drug carrier are that they afford NIR imaging with great penetration depths in biological tissues. In the meantime, they allow for selective uptake, accumulation and operation in biological samples.[61,62]

Metal nanoparticles such as Au and Ag are another type of commonly used constituent for constructing heterogeneous UCNPs. Metal nanoparticles can concentrate incident light and increase the excitation flux *via* a local electromagnetic field enhancement induced by surface plasmon resonance (SPR).[63,64] The near field effect also promotes radiative decay rates in UCNPs, thereby contributing to improved luminescence quantum yields.[65–68] However, quenching predominantly occurs if the UCNPs are brought into too close proximity of the metal surface due to the harmful Förster resonance energy transfer (FRET) effect.[69–74] Numerous experiments have shown that the enhancement of upconversion emission was maximized at a critical distance. In this regard, silica shells are typically employed as interlayers for tuning the distance between UCNPs and metallic nanostructures (Fig. 3e).[75] Silica displaying high optical transparency can form uniform shells on UCNPs with precisely controlled thickness from 2 to 100 nm.[76] Furthermore, silanol groups on the outer surface allow for the easy conjugation of metal nanoparticles through well-established silica surface chemistry.[77,78]

Although extensive investigations have been devoted to developing SPR enhanced upconversion, the resonance peaks of Au or Ag nanoparticles are typically in the long-wavelength region due to their intrinsic electronic configurations. Therefore, emission enhancement is typically observed for the green and red transitions.[66,79,80] To expand the range of SPR enhancement, Huang and co-workers recently developed a novel indium (In) structure to selectively enhance the blue upconversion emission in β-$NaYbF_4$:Tm UCNPs (Fig. 3f).[81] The β-$NaYbF_4$:Tm@SiO_2@In nanocomposites showed an almost 10-fold enhancement of upconversion luminescence at 450 nm upon 980 nm laser excitation, at an optimal working distance of 3 nm between the In nanoparticles and UCNPs.

Two-dimensional (2D) graphene and graphene-like nanomaterials such as graphene oxide (GO), layered transition metal dioxides (*e.g.*, MnO_2) and transition metal disulphides (*e.g.*, MoS_2) have attracted considerable attention as scaffolds for the assembly of UCNPs (Fig. 3g).[82–84] Due to their large specific surface area and strong optical absorption, these 2D nanomaterials have been employed as fluorescence quenchers of UCNPs for FRET assays.[85] The FRET systems are usually constructed by integrating bio-functionalised UCNPs to 2D nanosheets through physical interactions. Biomolecules like oligodeoxynucleotides (ODNs) and peptides can be physically adsorbed onto 2D nanosheets through π–π stacking interaction.[86,87] The interaction is significantly weakened when the ODNs form stable deoxyribonucleic acid (DNA) duplexes with target ODNs, which results in the disassembly of UCNP-2D materials and thus changes the optical properties of the FRET system.

It was also reported that some 2D nanomaterials such as MnO_2 nanosheets can be directly grown on UCNPs.[88] In 2018, we developed a facile method to couple MnO_2 nanosheets to core–satellite α-$NaYbF_4$@CaF_2 UCNPs (Fig. 3h).[30] The UCNPs were firstly modified with cetyl trimethylammonium bromide (CTAB), which served as a surfactant for surface functionalization. Then the CTAB-modified α-$NaYbF_4$:Tm@CaF_2 core–satellite UCNPs were used for the direct growth of MnO_2 nanosheets *via* electrostatic interactions. This surface modification method is expected to develop hybrids containing other types of 2D nanomaterials such as $Ni(OH)_2$ and MoS_2 nanosheets.[89,90]

3. Technological applications

The success in wet chemistry synthesis of Yb-based UCNPs with tunable size, morphology and hierarchical structure has largely enhanced the capability of upconversion. Owing to expanded optical tunability and improved emission performance, these Yb-based UCNPs offer exciting opportunities for emerging applications in the fields of biomedical science and photonics.

3.1. Biosensing

NIR excitation light induces negligible background fluorescence in biological samples. Biosensors incorporating UCNPs are thus rapidly emerging as outstanding candidates to rival traditional downshifting optical materials.[91–93] In many cases, however, the limit of detection (LOD) in UCNP-based sensors is constrained by unsatisfactory energy transfer performance, due to overlong separation or weak coupling between UCNPs and the reporters. In addition, conventional UCNPs such as $NaYF_4$:Yb/Er(Tm) with dominant green or blue emission become invalid when the analytes or the reporters in FRET systems prominently responded to ultraviolet (UV) light.

Yb-Based UCNPs typically feature strong multiphoton upconversion emission in the short-wavelength range and thus provide valuable additions to the toolbox of FRET sensors. We recently developed a biosensing platform by combining α-$NaYbF_4$:Tm (1 mol%)@CaF_2 core–satellite nanoparticles with MnO_2 nanosheets.[30] MnO_2 served as acceptors to quench UV emission from the UCNPs. The nanohybrids show recovered UV emissions upon the addition of glutathione (GSH), which efficiently degrades MnO_2 into soluble Mn^{2+} ions (Fig. 4a). This GSH probe with a LOD of 0.68 μM was proved to be superior to that composed of conventional β-$NaYF_4$:Yb/Tm@$NaYF_4$ core–shell UCNPs.[88]

Except for these Tm^{3+} activated UCNPs, strong UV emission was also achieved in Er^{3+}-activated KYb_2F_7 nanoparticles. The Yb-based host concentrates excitation energy that favours the

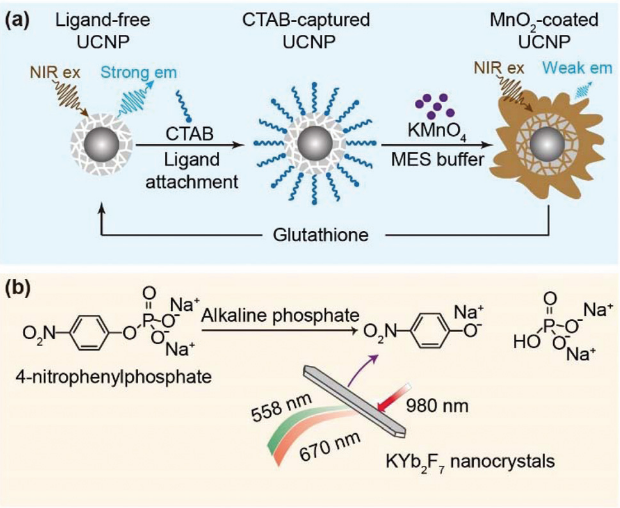

Fig. 4 Yb-Based UCNPs for biosensing. (a) Schematic design of surface modification and GSH detection by using the α-$NaYbF_4$:Tm (1 mol%)@CaF_2 core–satellite UCNPs. (b) Schematic design for screening the activity of alkaline phosphatase by using the KYb_2F_7 UCNPs. Reprinted with permission from ref. 30 and 33. Copyright 2018 the Royal Society of Chemistry and 2014 Springer Nature, respectively.

population of the $^2H_{9/2}$ state of Er^{3+} ions. Accordingly, a platform for enzyme sensing was developed by Liu and co-workers using fluorescent 4-nitrophenolate as the reporter, the absorption band of which fits well with the UV emission of Er^{3+} ions at around 400 nm.[33] The FRET sensor allows for screening alkaline phosphatases that catalyse the formation of 4-nitrophenolate (Fig. 4b). Alkaline phosphatases were commonly used to diagnose bone and hepatic diseases. The well-matched spectral overlap and reduced background fluorescence of Er^{3+}-activated KYb_2F_7 UCNPs result in the detection of enzyme concentration down to 1×10^{-5} U mg^{-1}.

3.2. Upconversion imaging and synergetic imaging

Bioimaging is of great significance in the study of pathological mechanism and clinical diagnosis of disease. Imaging techniques such as ultrasound imaging, magnetic resonance imaging, photoacoustic imaging, X-ray imaging and fluorescence imaging have been developed to visualize the structures of biological samples, analyte compositions and contents.[75] As a branch of fluorescence imaging, the upconversion imaging technique that uses NIR light as the excitation source offers deep penetration and weak autofluorescence for visualizing morphological details of sample species at the levels from living cells to small animals.[94–96]

Recent investigations suggested that $NaYbF_4$ UCNPs were more suitable than conventional $NaYF_4$ or $NaGdF_4$ for *in vitro* and *in vivo* bioimaging, due to their higher upconversion emission intensity at low excitation powers. In a representative example, Han and co-workers reported *in vivo* bioimaging using α-$NaYbF_4$:Tm (0.5 mol%)@CaF_2 core–shell UCNPs.[97] High-contrast imaging of deep tissues from the background was demonstrated by detecting the upconversion signal at 800 nm through the unshaved skin of a mouse (Fig. 5a). In a subsequent study, Damasco *et al.* further improved the ability for high contrast *in vivo* imaging by using phospholipid–polyethylene glycol (DSPE-PEG)-coated β-$NaYbF_4$:Tm@$NaYF_4$ core–shell UCNPs.[40]

Under 980 nm excitation, Er^{3+}-activated UCNPs usually show both upconversion (550 nm and 660 nm) and downshifting (~1550 nm) emissions, which could be utilized for synergetic downshifting NIR-II imaging.[98] NIR-II imaging (1000–1700 nm) affords high spatial resolution and deep-tissue penetration due to large Stokes shift and low scattering. Recently, Dai and co-workers developed a class of β-$NaYbF_4$:Er/Ce (2/2 mol%)@$NaYF_4$ core–shell nanoparticles for *in vivo* imaging.[99] These nanoparticles enabled fast *in vivo* imaging of blood vasculature in the mouse brain with a short exposure time in the NIR-II window (Fig. 5b). Such synergetic multi-mode imaging holds great promise in real-time monitoring and visualization of cerebrovascular abnormalities toward the diagnosis and therapy of the cerebral diseases.

Upconversion imaging with synergetic X-ray computed tomography (CT) in the recent decade emerged as a high-resolution and multi-dimensional imaging technique. Yb-Based UCNPs such as $NaYbF_4$ and $BaYbF_5$ UCNPs are appealing for these applications owing to the higher X-ray absorption coefficient of Yb than that of clinically used iobitridol (Yb: 3.88 cm^2 g^{-1} *vs.* iobitridol 1.94 cm^2 g^{-1} at 100 keV).[100,101] Lu and co-workers developed a β-$NaYbF_4$-based nanoparticulate CT contrast agent in 2012.[102] In their trial, a solution of PEG functionalized β-$NaYbF_4$ UCNPs was intravenously administered to a rat. The distribution of UCNPs was subsequently tracked by using an X-ray CT imaging system. A clear enhancement of the signal of the heart, liver, spleen and kidney was observed within 20 min (Fig. 5c). Particularly, the long-lasting liver-signal enhancement has great potential to improve the detection of the hepatic metastases.

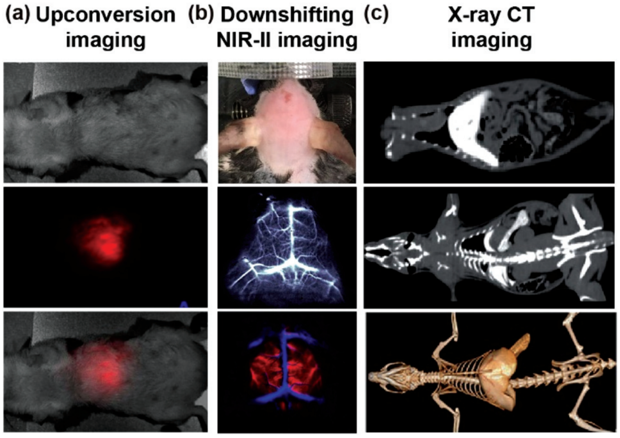

Fig. 5 Yb-Based UCNPs for upconversion imaging and synergetic imaging. (a) Whole-animal upconversion imaging of a BALB/c mouse injected with α-$NaYbF_4$:Tm^{3+} (0.5 mol%)@CaF_2 core–shell nanoparticles (excitation at 975 nm; emission at 800 nm). Top panel: Bright-field image; middle panel: upconversion image; bottom panel: merged image. (b) Synergetic downshifting NIR-II imaging of a C57Bl/6 mouse with hair shaved off. Top panel: Colour photograph; middle panel: cerebral vascular image; bottom panel: principal component analysis showing venous vessels (blue) and arterial vessels (red) (excitation at 980 nm; emission at 1550 nm). (c) *In vivo* CT coronal view images of a rat after intravenous injection of PEG-modified β-$NaYbF_4$:Er^{3+} nanoparticles. Top panel: Heart and liver CT imaging; middle panel: spleen and kidney CT imaging; bottom panel: the corresponding 3D rendering of the *in vivo* CT image. Reprinted with permission from ref. 97, 99 and 102. Copyright 2012 American Chemical Society, 2017 Springer Nature, 2012 WILEY-VCH Verlag GmbH & Co., respectively.

3.3. Upconversion optogenetics

Optogenetics involves the use of light to control light-sensitive ion channels in neurons. A commonly used light-gated ion channel protein is channelrhodopsin-2 (ChR2), which is activated by visible light in the blue range (~470 nm). The stimulation of ChR2 results in the opening of ion pores on the cellular membrane, which leads to the selective penetration of Na^+ and Ca^{2+} into the cytoplasm corresponding to a firing of neuronal impulse.[103,104] However, direct visible light excitation or fibre-guided insertion excitation will lead to either low stimulation efficiency or high tissue damage (Fig. 6a). As an alternative, upconversion-guided optogenetics, which uses UCNPs as the light transducer to transform highly penetrating NIR light into visible light *in situ*, is feasible for the manipu-

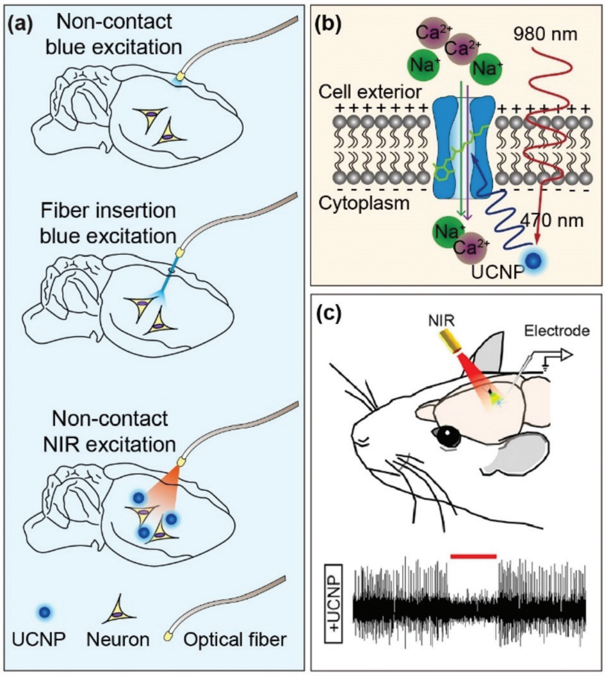

Fig. 6 Yb-Based UCNPs for applications in optogenetics. (a) Methods of sending light to deep-lying neurons in a mouse brain, including non-contact blue excitation, blue excitation through a surgically implanted optical fibre and noncontact NIR excitation through the use of UCNPs. (b) Schematic representation of optogenetic activation of neuronal signalling using β-$NaYbF_4$:Tm (0.5 mol%)@$NaYF_4$ core–shell UCNPs under 980 nm excitation. (c) *In vivo* neural stimulation using β-$NaYF_4$@$NaYbF_4$:Er (2 mol%)@$NaYF_4$ core–shell–shell UCNPs. Top panel: Schematics of NIR-optogenetic inhibition and extracellular recording in the brains of anesthetized animals; bottom panel: representative recordings of spiking activities in *eNpHR* neurons in response to excitation pulses of a 980 nm laser. Reprinted with permission from ref. 106–108. Copyright 2019 WILEY-VCH Verlag GmbH & Co., 2017 and 2018 American Chemical Society, respectively.

lation of neural tissues in a highly efficient and non-invasive manner.[105,106]

In a recent demonstration, Prasad and co-workers demonstrated the activation of the ChR2 channel for Ca^{2+} and Na^+ import by employing blue-emitting β-$NaYbF_4$:Tm (0.5 mol%)@$NaYF_4$ UCNPs as the nanotransducers.[107] The β-$NaYbF_4$:Tm (0.5 mol%)@$NaYF_4$ UCNPs were determined to be about six times brighter than conventional $NaYF_4$:Yb^{3+}/Tm^{3+} (30/0.5 mol%)@$NaYF_4$ UCNPs, thereby enabling the efficient activation of optogenetic proteins by 980 nm excitation at a low power density of ~5 W cm^{-2} (Fig. 6b). The study of optogenetics is expected to decode the complex organization of brain towards the design of novel therapeutics for the treatment of neurological disorders at the cellular level.

UCNP-based light transducers also allow for remote and *in vivo* neural inhibition. Shi and co-workers recently reported that the neural activities can be significantly inhibited and recovered by manipulating an implanted device containing highly emissive β-$NaYF_4$@$NaYbF_4$:Er^{3+} (2 mol%)@$NaYF_4$ UCNPs with 980 nm excitation at a power density of 0.6 W cm^{-2} (Fig. 6c).[108] By using the UCNP-based optogenetics device, fibre optics tethered to an animal's head is no longer needed, which is beneficial for chronic applications on freely moving animals.

3.4. Photoactivation

The concept of photoactivation derives from photosynthesis in which solar energy is absorbed by chlorophyll. Photoactivation is an effective approach in physics and biomedicine for photon conversion and manipulating the functions of biomolecules. For example, the β-$NaGdF_4$:Yb/Er@$NaYbF_4$@$NaNdF_4$@mSiO_2-PEG-RB nanocomposite emitted green light under the exposure of 808 nm irradiation, which activated the photosensitizer (RB) to produce reactive oxygen species (ROS) for killing cancer cells.[57] In another illustration, the blue-emitting UCNP@mSiO_2-Dox-azo nanohybrids triggered continuous wagging motions of the azobenzene molecules linked in the mesopore channels upon 980 nm laser irradiation, which propelled the release of anticancer drugs.[60] Notably, most photoactive receptors such as phytochromes show absorption maximum in the UV region. The photoactivation of these receptors is rather inefficient by conventional $NaYF_4$-based UCNPs with dominant emission in the visible region.[109–111]

To improve photoactivation efficiencies, Chen and co-workers developed a class of $LiYbF_4$:Tm (0.5 mol%)@$LiYF_4$ core–shell UCNPs as a versatile light source. The $LiYbF_4$-based UCNPs show intense UV emission at 362 nm, providing an efficient activation of a family of perovskite quantum dots (PeQDs) composed of $CsPbX_3$ (X = Cl, Br and I) (Fig. 7a).[112] The photoactivation process is dominated by a radiative energy transfer, in which upconverted UV light from the UCNPs was

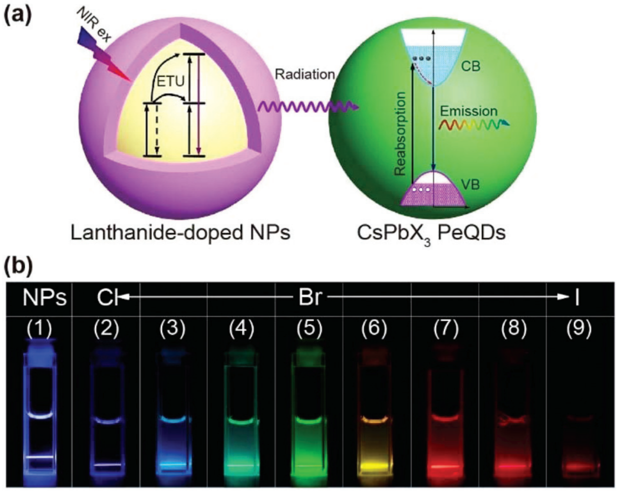

Fig. 7 Yb-Based UCNPs for photoactivation. (a) Schematic representation of the radiative energy transfer upconversion (RETU) processes in PeQDs through sensitization by $LiYbF_4$:Tm^{3+} (0.5 mol%)@$LiYF_4$ core–shell nanoparticles. (b) Photographs of multicolour emission through bandgap tailoring of PeQDs. Reprinted with permission from ref. 112. Copyright 2018 Springer Nature.

re-absorbed by the PeQDs. The tunable emission from the PeQDs is governed by the bandgap of PeQDs (Fig. 7b). In parallel with the benefits of high UV emission from Tm^{3+}-activated $LiYbF_4$ UCNPs and high UV absorption from PeQDs, this finding provides a general approach for generating photon upconversion in PeQDs under low power excitation and opens up a new avenue for multicolour imaging.

3.5. Upconversion lasing

Lasing in the UV range is highly desired for photonics, physics and biological applications. Upconversion is an attractive solution to realizing UV lasing by pumping with sophisticated long-wavelength lasers. In comparison with harmonic generations using nonlinear bulk crystals, UCNP-based lasing is readily obtained and tuned without the need for tight control of relative humidity, temperature and optical alignment.[113,114] Due to the lack of appropriate upconversion gain media, however, upconversion UV lasers were hardly realized for a long time in the past.[113]

To achieve intense UV emission through upconversion, our group designed a class of β-$NaYF_4$@$NaYbF_4$:Tm/Gd (1/30 mol%)@$NaYF_4$ core–shell–shell UCNPs (Fig. 8a). We found that the $NaYbF_4$ host in the mid-layer promotes population in the high-lying excited-state of Tm^{3+} activators by providing a high density of excitation energy (Fig. 8b).[28] Energy amassed in Tm^{3+} ions was subsequently transferred to Gd^{3+} dopants that generated emission at ~310 nm featuring sharp bandwidth and long lifetime (Fig. 8c). Using these UV-emitting UCNPs as gain media in a bottle-like microcavity, we obtained deep UV lasing at 310.5 nm by excitation in the NIR at 980 nm (Fig. 8d). Notably, this was the first demonstration that the silica resin microcavity supports upconversion UV lasing emission through the formation of whispering gallery modes (WGMs). WGMs refer to circular optical modes in resonators, in which the closed trajectories of light are supported by total internal reflections from boundaries of the curved and polygonal transparent dielectric structures, such as a ring, a cylinder, a disk or a sphere.[115–118]

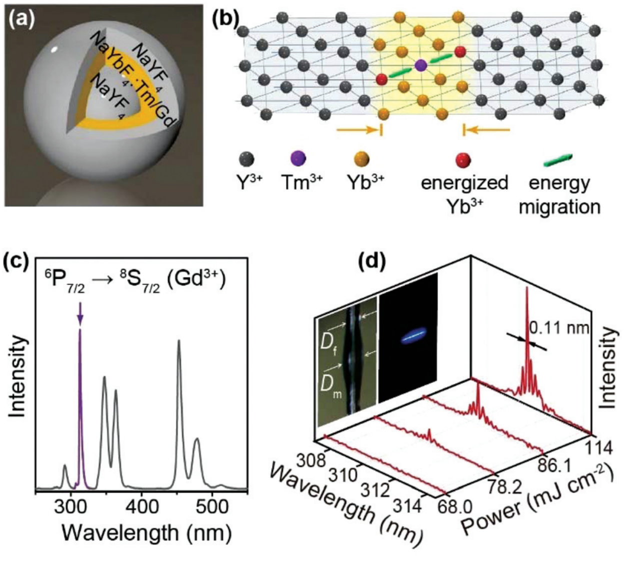

Fig. 8 Yb-Based UCNPs for upconversion lasing. (a) Schematic design of sandwich-structured β-$NaYF_4$@$NaYbF_4$:Tm^{3+}/Gd^{3+} (1/30 mol%)@$NaYF_4$ UCNPs. (b) Schematic illustration of energy transfer from Yb^{3+} to Tm^{3+} in the Yb-sublattice. (c) Emission spectrum of the β-$NaYF_4$@$NaYbF_4$:Tm^{3+}/Gd^{3+} (1/30 mol%)@$NaYF_4$ UCNPs under 980 nm excitation. (d) Lasing spectra of the micro-resonator containing the β-$NaYF_4$@$NaYbF_4$:Tm^{3+}/Gd^{3+} (1/30 mol%)@$NaYF_4$ UCNPs as gain media under excitation of 980 nm at different power densities. Insets: Photographs of the micro-resonator without and with optical excitation. D_f and D_m denote diameters of the support fibre and microcavity, respectively. Reprinted with permission from ref. 28. Copyright 2016 Springer Nature.

In a further development, Jin and co-workers realized ultraviolet B (UVB) microlasers with high gain coefficient at 288.6 nm by using $LiYbF_4$:Tm@$LiYbF_4$@$LiLuF_4$ UCNPs as the gain media.[119] The inner $LiYbF_4$ shell was designed to enhance the absorption of excitation light and subsequent energy transfer to Tm^{3+} activators. UVB lasing was also enabled by the microcavity composed of a UCNP-on-SiO_2 microdisk, which maximizes optical output at 288.6 nm by limiting emissions at longer wavelengths such as 345 and 361 nm. The UCNP-based UV microlasers are highly reproducible, thereby holding great promise in revolutionizing the fabrication of cost effective and compact deep UV lasers.

3.6. Anti-counterfeiting

Anti-counterfeiting technologies based on covert luminescent patterns are widely used in paper currencies, product trademarks, identity cards and important certificates.[120,121] UCNPs are advantageous for anti-counterfeiting applications due to their high chemical stability as well as great optical tunability. By appropriate doping, UCNPs can be made to produce multicolour emission by single-wavelength excitation or by alteration of excitation conditions, which can be harnessed to encrypt anti-counterfeiting patterns with a large encoding capacity.[122–126]

The emission spectra of Yb-based UCNPs typically show strong dependence on excitation power due to the highly efficient excitation process, which accelerates the saturation of upconversion emissions. Therefore, colour codes are easily achieved in Yb-based UCNPs by the manipulation of excitation power. For example, we attained a wide tunability of the red-to-green emission intensity ratio from 0.37 to 5.19 in a Ho^{3+}-activated β-$NaYbF_4$ UCNPs by increasing the excitation power from 1.25 to 46.25 W cm^{-2} (Fig. 9a).[49] By contrast, excitation power variation in the same range only induces a marginal colour shift in Yb/Ho-codoped $NaYF_4$ UCNPs. In another work, Chen and co-workers achieved emission colour tuning from green to red in β-$NaYbF_4$:Er (2 mol%)@$NaYF_4$ core–shell UCNPs by increasing the excitation power density from 0.1 to 4.0 W cm^{-2}.[127] The Yb-based UCNPs were used to encrypt security labels on trademark tags and painting in conjunction with conventional $NaYF_4$:Yb/Er UCNPs as a reference. A genuine pattern shows prescribed colour changes by excitation at varying powers (Fig. 9b).

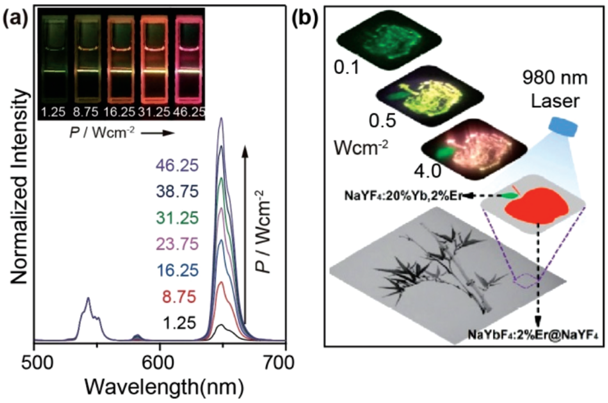

Fig. 9 Yb-Based UCNPs for multicolour encoding and anti-counterfeiting. (a) Normalized emission spectra of the β-$NaYF_4$@$NaYbF_4$:Ho (1 mol%)@$NaYF_4$ UCNPs under 980 nm excitation at varying power densities. Insets: Luminescence photos of the corresponding samples. (b) Luminescence image of the anti-counterfeiting pattern composed of β-$NaYbF_4$:Er (2 mol%)@$NaYF_4$ UCNPs under excitation of 980 nm at different powers. Reprinted with permission from ref. 49 and 127. Copyright 2016 American Chemical Society and 2019 Tsinghua University Press and Springer-Verlag GmbH Germany, part of Springer Nature, respectively.

4. Conclusions

This review has discussed the recent development of Yb-based fluoride UCNPs. With significant progress made over the past few years, high-quality Yb-based UCNPs of well-defined size and structure can be precisely synthesized to produce intense and tunable emission spanning UV to NIR. Methods for integrating these UCNPs with other types of nanostructured building blocks are also established. The resulting nanohybrids have shown great promise in technological applications such as biological sensing, upconversion lasing and anti-counterfeiting. To realize the full potential of Yb-based upconversion, new hosts of diverse compositions and crystal structures doped with high concentrations of lanthanide activators should be explored. In addition, detailed energy transfer processes, especially back-energy-transfer from upconverting activators to Yb^{3+} sensitizers, should be carefully studied in order to further enhance upconversion emissions and to create novel upconversion properties. The continuous development of Yb-based UCNPs is expected to push forward the frontiers of upconversion research in the future.

Conflicts of interest

There are no conflicts of interest to declare.

Acknowledgements

This work was supported by the National Natural Science Foundation of China (No. 21573185 and 21773200) and the Research Grants Council of Hong Kong (CityU 11204717 and 11205219).

References

1 H. Dong, L.-D. Sun and C.-H. Yan, Energy transfer in lanthanide upconversion studies for extended optical applications, *Chem. Soc. Rev.*, 2015, **44**, 1608–1634.
2 J. C. Goldschmidt and S. Fischer, Upconversion for photovoltaics–a review of materials, devices and concepts for performance enhancement, *Adv. Opt. Mater.*, 2015, **3**, 510–535.
3 Y. I. Park, K. T. Lee, Y. D. Suh and T. Hyeon, Upconverting nanoparticles: a versatile platform for wide-field two-photon microscopy and multi-modal in vivo imaging, *Chem. Soc. Rev.*, 2015, **44**, 1302–1317.
4 T. F. Schulze and T. W. Schmidt, Photochemical upconversion: present status and prospects for its application to solar energy conversion, *Energy Environ. Sci.*, 2015, **8**, 103–125.
5 M.-K. Tsang, G. Bai and J. Hao, Stimuli responsive upconversion luminescence nanomaterials and films for various applications, *Chem. Soc. Rev.*, 2015, **44**, 1585–1607.
6 W. Zheng, P. Huang, D. Tu, E. Ma, H. Zhu and X. Chen, Lanthanide-doped upconversion nano-bioprobes: electronic structures, optical properties, and biodetection, *Chem. Soc. Rev.*, 2015, **44**, 1379–1415.
7 X. Chen, D. Peng, Q. Ju and F. Wang, Photon upconversion in core–shell nanoparticles, *Chem. Soc. Rev.*, 2015, **44**, 1318–1330.
8 B. del Rosal and D. Jaque, Upconversion nanoparticles for in vivo applications: limitations and future perspectives, *Methods Appl. Fluoresc.*, 2019, **7**, 022001.
9 J. C. G. Bünzli, Lanthanide photonics: shaping the nanoworld, *Trends Chem.*, 2019, **1**, 751–762.
10 Y. I. Park, K. T. Lee, Y. D. Suh and T. Hyeon, Upconverting nanoparticles: a versatile platform for wide-field two-photon microscopy and multi-modal in vivo imaging, *Chem. Soc. Rev.*, 2015, **44**, 1302–1317.
11 M. K. Mahata, H. Bae and K. T. Lee, Upconversion luminescence sensitized pH-nanoprobes, *Molecules*, 2017, **22**, 2064.
12 K. Shin, Y. H. Song, Y. Goh and K. T. Lee, Two-dimensional and three-dimensional single particle tracking of upconverting nanoparticles in living cells, *Int. J. Mol. Sci.*, 2019, **20**, 1424.
13 S. Wen, J. Zhou, P. J. Schuck, Y. D. Suh, T. W. Schmidt and D. Jin, Future and challenges for hybrid upconversion nanosystems, *Nat. Photonics*, 2019, **13**, 828.
14 S. Wen, J. Zhou, K. Zheng, A. Bednarkiewicz, X. Liu and D. Jin, Advances in highly doped upconversion nanoparticles, *Nat. Commun.*, 2018, **9**, 2415.
15 D. A. Hirsh, N. J. Johnson, F. C. van Veggel and R. W. Schurko, Local structure of rare-earth fluorides in

bulk and core/shell nanocrystalline materials, *Chem. Mater.*, 2015, **27**, 6495–6507.

16 J.-C. Boyer, F. Vetrone, L. A. Cuccia and J. A. Capobianco, Synthesis of colloidal upconverting $NaYF_4$ nanocrystals doped with Er^{3+}, Yb^{3+} and Tm^{3+}, Yb^{3+} via thermal decomposition of lanthanide trifluoroacetate precursors, *J. Am. Chem. Soc.*, 2006, **128**, 7444–7445.

17 S. Fischer, N. D. Bronstein, J. K. Swabeck, E. M. Chan and A. P. Alivisatos, Precise tuning of surface quenching for luminescence enhancement in core–shell lanthanide-doped nanocrystals, *Nano Lett.*, 2016, **16**, 7241–7247.

18 M. Haase and H. Schäfer, Upconverting nanoparticles, *Angew. Chem., Int. Ed.*, 2011, **50**, 5808–5829.

19 H.-X. Mai, Y.-W. Zhang, L.-D. Sun and C.-H. Yan, Highly efficient multicolor up-conversion emissions and their mechanisms of monodisperse $NaYF_4$: Yb, Er core and core/shell-structured nanocrystals, *J. Phys. Chem. C*, 2007, **111**, 13721–13729.

20 L. Wang and Y. Li, Controlled synthesis and luminescence of lanthanide doped $NaYF_4$ nanocrystals, *Chem. Mater.*, 2007, **19**, 727–734.

21 F. Wang and X. Liu, Recent advances in the chemistry of lanthanide-doped upconversion nanocrystals, *Chem. Soc. Rev.*, 2009, **38**, 976–989.

22 B. Zhou, B. Shi, D. Jin and X. Liu, Controlling upconversion nanocrystals for emerging applications, *Nat. Nanotechnol.*, 2015, **10**, 924–936.

23 B. Chen and F. Wang, Combating concentration quenching in upconversion nanoparticles, *Acc. Chem. Res.*, 2019, DOI: 10.1021/acs.accounts.9b00453.

24 D. J. Gargas, E. M. Chan, A. D. Ostrowski, S. Aloni, M. V. P. Altoe, E. S. Barnard, B. Sanii, J. J. Urban, D. J. Milliron, B. E. Cohen and P. J. Schuck, Engineering bright sub-10-nm upconverting nanocrystals for single-molecule imaging, *Nat. Nanotechnol.*, 2014, **9**, 300–305.

25 X. Wang, R. R. Valiev, T. Y. Ohulchanskyy, H. Ågren, C. Yang and G. Chen, Dye-sensitized lanthanide-doped upconversion nanoparticles, *Chem. Soc. Rev.*, 2017, **46**, 4150–4167.

26 J. Zhao, D. Jin, E. P. Schartner, Y. Lu, Y. Liu, A. V. Zvyagin, L. Zhang, J. M. Dawes, P. Xi, J. A. Piper, E. M. Goldys and T. M. Monro, Single-nanocrystal sensitivity achieved by enhanced upconversion luminescence, *Nat. Nanotechnol.*, 2013, **8**, 729–734.

27 W. Zou, C. Visser, J. A. Maduro, M. S. Pshenichnikov and J. C. Hummelen, Broadband dye-sensitized upconversion of near-infrared light, *Nat. Photonics*, 2012, **6**, 560–564.

28 X. Chen, L. Jin, W. Kong, T. Sun, W. Zhang, X. Liu, J. Fan, S. F. Yu and F. Wang, Confining energy migration in upconversion nanoparticles towards deep ultraviolet lasing, *Nat. Commun.*, 2016, **7**, 10304.

29 B. Chen, W. Kong, N. Wang, G. Zhu and F. Wang, Oleylamine-mediated synthesis of small $NaYbF_4$ nanoparticles with tunable size, *Chem. Mater.*, 2019, **31**, 4779–4786.

30 B. Chen and F. Wang, $NaYbF_4$@CaF_2 core–satellite upconversion nanoparticles: one-pot synthesis and sensitive detection of glutathione, *Nanoscale*, 2018, **10**, 19898–19905.

31 Y. Liu, K. Ai, J. Liu, Q. Yuan, Y. He and L. Lu, Hybrid $BaYbF_5$ nanoparticles: novel binary contrast agent for high-resolution *in vivo* X-ray computed tomography angiography, *Adv. Healthcare Mater.*, 2012, **1**, 461–466.

32 Z. Liu, E. Ju, J. Liu, Y. Du, Z. Li, Q. Yuan, J. Ren and X. Qu, Direct visualization of gastrointestinal tract with lanthanide-doped $BaYbF_5$ upconversion nanoprobes, *Biomaterials*, 2013, **34**, 7444–7452.

33 J. Wang, R. Deng, M. A. MacDonald, B. Chen, J. Yuan, F. Wang, D. Chi, T. S. A. Hor, P. Zhang and X. Liu, Enhancing multiphoton upconversion through energy clustering at sublattice level, *Nat. Mater.*, 2014, **13**, 157–162.

34 Q. Zou, P. Huang, W. Zheng, W. You, R. Li, D. Tu, J. Xu and X. Chen, Cooperative and non-cooperative sensitization upconversion in lanthanide-doped $LiYbF_4$ nanoparticles, *Nanoscale*, 2017, **9**, 6521–6528.

35 F. Wang, R. Deng and X. Liu, Preparation of core–shell $NaGdF_4$ nanoparticles doped with luminescent lanthanide ions to be used as upconversion-based probes, *Nat. Protoc.*, 2014, **9**, 1634–1644.

36 R. Naccache, Q. Yu and J. A. Capobianco, The fluoride host: nucleation, growth, and upconversion of lanthanide-doped nanoparticles, *Adv. Opt. Mater.*, 2015, **3**, 482–509.

37 B. Chen, B. Ren and F. Wang, Cs^+-assisted synthesis of $NaLaF_4$ nanoparticles, *Chem. Mater.*, 2019, **31**, 9497.

38 B. Zhou, W. Yang, S. Han, Q. Sun and X. Liu, Photon upconversion through Tb^{3+}-mediated interfacial energy transfer, *Adv. Mater.*, 2015, **27**, 6208–6212.

39 F. Wang, Y. Han, C. S. Lim, Y. Lu, J. Wang, J. Xu, H. Chen, C. Zhang, M. Hong and X. Liu, Simultaneous phase and size control of upconversion nanocrystals through lanthanide doping, *Nature*, 2010, **463**, 1061–1065.

40 J. A. Damasco, G. Chen, W. Shao, H. Ågren, H. Huang, W. Song, J. F. Lovell and P. N. Prasad, Size-tunable and monodisperse Tm^{3+}/Gd^{3+}-doped hexagonal $NaYbF_4$ nanoparticles with engineered efficient near infrared-to-near infrared upconversion for in vivo imaging, *ACS Appl. Mater. Interfaces*, 2014, **6**, 13884–13893.

41 C. Ma, X. Xu, F. Wang, Z. Zhou, D. Liu, J. Zhao, M. Guan, C. I. Lang and D. Jin, Optimal sensitizer concentration in single upconversion nanocrystals, *Nano Lett.*, 2017, **17**, 2858–2864.

42 B. Chen, D. Peng, X. Chen, X. Qiao, X. Fan and F. Wang, Establishing the structural integrity of core–shell nanoparticles against elemental migration using luminescent lanthanide probes, *Angew. Chem., Int. Ed.*, 2015, **54**, 12788–12790.

43 D. Hudry, D. Busko, R. Popescu, D. Gerthsen, A. M. Abeykoon, C. Kübel, T. Bergfeldt and B. S. Richards, Direct evidence of significant cation intermixing in upconverting core@shell nanocrystals: Toward a new crystallochemical model, *Chem. Mater.*, 2017, **29**, 9238–9246.

44 L. Liu, X. Li, Y. Fan, C. Wang, A. M. El-Toni, M. S. Alhoshan, D. Zhao and F. Zhang, Elemental migration in core/shell structured lanthanide doped nanoparticles, *Chem. Mater.*, 2019, **31**, 5608–5615.

45 R. Shi, X. Ling, X. Li, L. Zhang, M. Lu, X. Xie, L. Huang and W. Huang, Tuning hexagonal $NaYbF_4$ nanocrystals down to sub-10 nm for enhanced photon upconversion, *Nanoscale*, 2017, **9**, 13739–13746.

46 T. Cheng, R. Marin, A. Skripka and F. Vetrone, Small and bright lithium-based upconverting nanoparticles, *J. Am. Chem. Soc.*, 2018, **140**, 12890–12899.

47 B. Shen, S. Cheng, Y. Gu, D. Ni, Y. Gao, Q. Su, W. Feng and F. Li, Revisiting the optimized doping ratio in core/shell nanostructured upconversion particles, *Nanoscale*, 2017, **9**, 1964–1971.

48 G. Chen, H. Ågren, T. Y. Ohulchanskyy and P. N. Prasad, Light upconverting core–shell nanostructures: nanophotonic control for emerging applications, *Chem. Soc. Rev.*, 2015, **44**, 1680–1713.

49 B. Chen, Y. Liu, Y. Xiao, X. Chen, Y. Li, M. Li, X. Qiao, X. Fan and F. Wang, Amplifying excitation-power sensitivity of photon upconversion in a $NaYbF_4$: Ho nanostructure for direct visualization of electromagnetic hotspots, *J. Phys. Chem. Lett.*, 2016, **7**, 4916–4921.

50 H. Wen, H. Zhu, X. Chen, T. F. Hung, B. Wang, G. Zhu, S. F. Yu and F. Wang, Upconverting near-infrared light through energy management in core–shell–shell nanoparticles, *Angew. Chem., Int. Ed.*, 2013, **52**, 13419–13423.

51 B. del Rosal, U. Rocha, E. Ximendes, E. M. Rodríguez, D. Jaque and J. G. Solé, Nd^{3+} ions in nanomedicine: Perspectives and applications, *Opt. Mater.*, 2017, **63**, 185–196.

52 X. Xie, Z. Li, Y. Zhang, S. Guo, A. I. Pendharkar, M. Lu, L. Huang, W. Huang and G. Han, Emerging ≈ 800 nm excited lanthanide-doped upconversion nanoparticles, *Small*, 2017, **13**, 1602843.

53 X. Li, F. Zhang and D. Zhao, Lab on upconversion nanoparticles: optical properties and applications engineering via designed nanostructure, *Chem. Soc. Rev.*, 2015, **44**, 1346–1378.

54 K. Deng, C. Li, S. Huang, B. Xing, D. Jin, Q. Zeng, Z. Hou and J. Lin, Recent progress in near infrared light triggered photodynamic therapy, *Small*, 2017, **13**, 1702299.

55 F. Lu, L. Yang, Y. Ding and J. J. Zhu, Highly emissive Nd^{3+}-sensitized multilayered upconversion nanoparticles for efficient 795 nm operated photodynamic therapy, *Adv. Funct. Mater.*, 2016, **26**, 4778–4785.

56 G. Yang, D. Yang, P. Yang, R. Lv, C. Li, C. Zhong, F. He, S. Gai and J. Lin, A single 808 nm near-infrared light-mediated multiple imaging and photodynamic therapy based on titania coupled upconversion nanoparticles, *Chem. Mater.*, 2015, **27**, 7957–7968.

57 J. Li, J. Huang, Y. Ao, S. Li, Y. Miao, Z. Yu, L. Zhu, X. Lan, Y. Zhu, Y. Zhang and X. Yang, Synergizing upconversion nanophotosensitizers with hyperbaric oxygen to remodel the extracellular matrix for enhanced photodynamic cancer therapy, *ACS Appl. Mater. Interfaces*, 2018, **10**, 22985–22996.

58 W. Fan, W. Bu, B. Shen, Q. He, Z. Cui, Y. Liu, X. Zheng, K. Zhao and J. Shi, Intelligent MnO_2 nanosheets anchored with upconversion nanoprobes for concurrent pH-/H_2O_2-responsive UCL imaging and oxygen-elevated synergetic therapy, *Adv. Mater.*, 2015, **27**, 4155–4161.

59 A. Punjabi, X. Wu, A. Tokatli-Apollon, M. El-Rifai, H. Lee, Y. Zhang, C. Wang, Z. Liu, E. M. Chan, C. Duan and G. Han, Amplifying the red-emission of upconverting nanoparticles for biocompatible clinically used prodrug-induced photodynamic therapy, *ACS Nano*, 2014, **8**, 10621–10630.

60 J. Liu, W. Bu, L. Pan and J. Shi, NIR-triggered anticancer drug delivery by upconverting nanoparticles with integrated azobenzene-modified mesoporous silica, *Angew. Chem., Int. Ed.*, 2013, **52**, 4375–4379.

61 C. Gao, Z. Lin, Z. Wu, X. Lin and Q. He, Stem-cell-membrane camouflaging on near-infrared photoactivated upconversion nanoarchitectures for in vivo remote-controlled photodynamic therapy, *ACS Appl. Mater. Interfaces*, 2016, **8**, 34252–34260.

62 S. Wilhelm, Perspectives for upconverting nanoparticles, *ACS Nano*, 2017, **11**, 10644–10653.

63 L. He, M. D. Musick, S. R. Nicewarner, F. G. Salinas, S. J. Benkovic, M. J. Natan and C. D. Keating, Colloidal Au-enhanced surface plasmon resonance for ultrasensitive detection of DNA hybridization, *J. Am. Chem. Soc.*, 2000, **122**, 9071–9077.

64 D. Schaadt, B. Feng and E. Yu, Enhanced semiconductor optical absorption via surface plasmon excitation in metal nanoparticles, *Appl. Phys. Lett.*, 2005, **86**, 063106.

65 S. Fischer, F. Hallermann, T. Eichelkraut, G. von Plessen, K. W. Krämer, D. Biner, H. Steinkemper, M. Hermle and J. C. Goldschmidt, Plasmon enhanced upconversion luminescence near gold nanoparticles–simulation and analysis of the interactions, *Opt. Express*, 2012, **20**, 271–282.

66 M. Saboktakin, X. Ye, U. K. Chettiar, N. Engheta, C. B. Murray and C. R. Kagan, Plasmonic enhancement of nanophosphor upconversion luminescence in Au nanohole arrays, *ACS Nano*, 2013, **7**, 7186–7192.

67 S. Schietinger, T. Aichele, H.-Q. Wang, T. Nann and O. Benson, Plasmon-enhanced upconversion in single $NaYF_4$: Yb^{3+}/Er^{3+} codoped nanocrystals, *Nano Lett.*, 2009, **10**, 134–138.

68 D. M. Wu, A. García-Etxarri, A. Salleo and J. A. Dionne, Plasmon-enhanced upconversion, *J. Phys. Chem. Lett.*, 2014, **5**, 4020–4031.

69 T. Förster, Zwischenmolekulare Energiewanderung und Fluoreszenz, *Ann. Phys.*, 1948, **2**, 55–75.

70 R. M. Clegg, Förster resonance energy transfer—FRET what is it, why do it, and how it's done, *Lab. Tech. Biochem. Mol. Biol.*, 2009, **33**, 1–57.

71 H. Xing, T. Wei, X. Lin and Z. Dai, Near-infrared MnCuInS/ZnS@ BSA and urchin-like Au nanoparticle as a

novel donor-acceptor pair for enhanced FRET biosensing, *Anal. Chim. Acta*, 2018, **1042**, 71–78.

72 L. Tang, S. Mo, S. G. Liu, Y. Ling, X. F. Zhang, N. B. Li and H. Q. Luo, A sensitive "Turn-On" fluorescent sensor for melamine based on FRET effect between polydopamine-glutathione nanoparticles and Ag nanoparticles, *J. Agric. Food Chem.*, 2018, **66**, 2174–2179.

73 J. Wang, F. Cao, S. He, Y. Xia, X. Liu, W. Jiang, Y. Yu, H. Zhang and W. Chen, FRET on lateral flow test strip to enhance sensitivity for detecting cancer biomarker, *Talanta*, 2018, **176**, 444–449.

74 Y. Wu, J. Xu, E. T. Poh, L. Liang, H. Liu, J. K. W. Yang, C. W. Qiu, R. A. L. Vallée and X. Liu, Upconversion superburst with sub-2μs lifetime, *Nat. Nanotechnol.*, 2019, **14**, 1110.

75 J. He, W. Zheng, F. Ligmajer, C.-F. Chan, Z. Bao, K.-L. Wong, X. Chen, J. Hao, J. Dai, S.-F. Yu and D. Y. Lei, Plasmonic enhancement and polarization dependence of nonlinear upconversion emissions from single gold nanorod@ SiO_2@CaF_2: Yb^{3+}, Er^{3+} hybrid core–shell–satellite nanostructures, *Light: Sci. Appl.*, 2017, **6**, e16217.

76 J.-N. Liu, W.-B. Bu and J.-L. Shi, Silica coated upconversion nanoparticles: A versatile platform for the development of efficient theranostics, *Acc. Chem. Res.*, 2015, **48**, 1797–1805.

77 X. Chen, D. Zhou, W. Xu, J. Zhu, G. Pan, Z. Yin, H. Wang, Y. Zhu, C. Shaobo and H. Song, Fabrication of Au-Ag nanocage@$NaYF_4$@$NaYF_4$: Yb, Er core–shell hybrid and its tunable upconversion enhancement, *Sci. Rep.*, 2017, **7**, 41079.

78 F. Kang, J. He, T. Sun, Z. Y. Bao, F. Wang and D. Y. Lei, Plasmonic dual-enhancement and precise color tuning of gold nanorod@SiO_2 coupled core–shell–shell upconversion nanocrystals, *Adv. Funct. Mater.*, 2017, **27**, 1701842.

79 X. Chen, W. Xu, L. Zhang, X. Bai, S. Cui, D. Zhou, Z. Yin, H. Song and D. H. Kim, Large upconversion enhancement in the "Islands" Au–Ag Alloy/$NaYF_4$: Yb^{3+}, Tm^{3+}/Er^{3+} composite films, and fingerprint identification, *Adv. Funct. Mater.*, 2015, **25**, 5462–5471.

80 D. Lu, S. K. Cho, S. Ahn, L. Brun, C. J. Summers and W. Park, Plasmon enhancement mechanism for the upconversion processes in $NaYF_4$: Yb^{3+}, Er^{3+} nanoparticles: Maxwell versus Förster, *ACS Nano*, 2014, **8**, 7780–7792.

81 L. Wang, S. Guo, D. Liu, J. He, J. Zhou, K. Zhang, Y. Wei, Y. Pan, C. Gao, Z. Yuan, D. Lei, X. Xie and L. Huang, Plasmon-enhanced blue upconversion luminescence by indium nanocrystals, *Adv. Funct. Mater.*, 2019, **29**, 1901242.

82 Y. Wang, H. Wang, D. Liu, S. Song, X. Wang and H. Zhang, Graphene oxide covalently grafted upconversion nanoparticles for combined NIR mediated imaging and photothermal/photodynamic cancer therapy, *Biomaterials*, 2013, **34**, 7715–7724.

83 J. Yuan, Y. Cen, X.-J. Kong, S. Wu, C.-L. Liu, R.-Q. Yu and X. Chu, MnO_2-nanosheet-modified upconversion nanosystem for sensitive turn-on fluorescence detection of H_2O_2 and glucose in blood, *ACS Appl. Mater. Interfaces*, 2015, **7**, 10548–10555.

84 L. Zhou, X. Zheng, Z. Gu, W. Yin, X. Zhang, L. Ruan, Y. Yang, Z. Hu and Y. Zhao, Mesoporous $NaYbF_4$@$NaGdF_4$ core–shell up-conversion nanoparticles for targeted drug delivery and multimodal imaging, *Biomaterials*, 2014, **35**, 7666–7678.

85 F. Tian, J. Lyu, J. Shi and M. Yang, Graphene and graphene-like two-denominational materials based fluorescence resonance energy transfer (FRET) assays for biological applications, *Biosens. Bioelectron.*, 2017, **89**, 123–135.

86 C. Chung, Y.-K. Kim, D. Shin, S.-R. Ryoo, B. H. Hong and D.-H. Min, Biomedical applications of graphene and graphene oxide, *Acc. Chem. Res.*, 2013, **46**, 2211–2224.

87 E. Morales-Narváez and A. Merkoçi, Graphene oxide as an optical biosensing platform, *Adv. Mater.*, 2012, **24**, 3298–3308.

88 R. Deng, X. Xie, M. Vendrell, Y.-T. Chang and X. Liu, Intracellular glutathione detection using MnO_2-nanosheet-modified upconversion nanoparticles, *J. Am. Chem. Soc.*, 2011, **133**, 20168–20171.

89 X. Xu, Y. Long, P. Lei, L. Dong, K. Du, J. Feng and H. Zhang, A pH-responsive assembly based on upconversion nanocrystals and ultrasmall nickel nanoparticles, *J. Mater. Chem. C*, 2017, **5**, 9666–9672.

90 Y. Zhai, X. Yang, F. Wang, Z. Li, G. Ding, Z. Qiu, Y. Wang, Y. Zhou and S. T. Han, Infrared-sensitive memory based on direct-grown MoS_2-upconversion-nanoparticle heterostructure, *Adv. Mater.*, 2018, **30**, 1803563.

91 B. Chen, Q. Su, W. Kong, Y. Wang, P. Shi and F. Wang, Energy transfer-based biodetection using optical nanomaterials, *J. Mater. Chem. B*, 2018, **6**, 2924–2944.

92 N. Hildebrandt, C. M. Spillmann, W. R. Algar, T. Pons, M. H. Stewart, E. Oh, K. Susumu, S. A. Diaz, J. B. Delehanty and I. L. Medintz, Energy transfer with semiconductor quantum dot bioconjugates: a versatile platform for biosensing, energy harvesting, and other developing applications, *Chem. Rev.*, 2016, **117**, 536–711.

93 J. Wen, Y. Xu, H. Li, A. Lu and S. Sun, Recent applications of carbon nanomaterials in fluorescence biosensing and bioimaging, *Chem. Commun.*, 2015, **51**, 11346–11358.

94 S. A. Hilderbrand and R. Weissleder, Near-infrared fluorescence: application to in vivo molecular imaging, *Curr. Opin. Chem. Biol.*, 2010, **14**, 71–79.

95 J. Rieffel, F. Chen, J. Kim, G. Chen, W. Shao, S. Shao, U. Chitgupi, R. Hernandez, S. A. Graves, R. J. Nickles and P. N. Prasad, Hexamodal imaging with porphyrin-phospholipid-coated upconversion nanoparticles, *Adv. Mater.*, 2015, **27**, 1785–1790.

96 J. Zhou, Z. Liu and F. Li, Upconversion nanophosphors for small-animal imaging, *Chem. Soc. Rev.*, 2012, **41**, 1323–1349.

97 G. Chen, J. Shen, T. Y. Ohulchanskyy, N. J. Patel, A. Kutikov, Z. Li, J. Song, R. K. Pandey, H. Ågren,

P. N. Prasad and G. Han, (α-NaYbF$_4$: Tm^{3+})/CaF$_2$ core/shell nanoparticles with efficient near-infrared to near-infrared upconversion for high-contrast deep tissue bioimaging, *ACS Nano*, 2012, **6**, 8280–8287.

98 Y. Zhong, Z. Ma, F. Wang, X. Wang, Y. Yang, Y. Liu, X. Zhao, J. Li, H. Du, M. Zhang, Q. Cui, S. Zhu, Q. Sun, H. Wan, Y. Tian, Q. Liu, W. Wang, K. C. Garcia and H. Dai, In vivo molecular imaging for immunotherapy using ultra-bright near-infrared-IIb rare-earth nanoparticles, *Nat. Biotechnol.*, 2019, **37**, 1322–1331.

99 Y. Zhong, Z. Ma, S. Zhu, J. Yue, M. Zhang, A. L. Antaris, J. Yuan, R. Cui, H. Wan, Y. Zhou, W. Wang, N. F. Huang, J. Luo, Z. Hu and H. Dai, Boosting the down-shifting luminescence of rare-earth nanocrystals for biological imaging beyond 1500 nm, *Nat. Commun.*, 2017, **8**, 737.

100 G. Tian, X. Zheng, X. Zhang, W. Yin, J. Yu, D. Wang, Z. Zhang, X. Yang, Z. Gu and Y. Zhao, TPGS-stabilized NaYbF$_4$:Er upconversion nanoparticles for dual-modal fluorescent/CT imaging and anticancer drug delivery to overcome multi-drug resistance, *Biomaterials*, 2015, **40**, 107–116.

101 Z. Yi, S. Zeng, W. Lu, H. Wang, L. Rao, H. Liu and J. Hao, Synergistic dual-modality in vivo upconversion luminescence/X-ray imaging and tracking of amine-functionalized NaYbF$_4$: Er nanoprobes, *ACS Appl. Mater. Interfaces*, 2014, **6**, 3839–3846.

102 Y. Liu, K. Ai, J. Liu, Q. Yuan, Y. He and L. Lu, A high-performance ytterbium-based nanoparticulate contrast agent for in vivo X-ray computed tomography imaging, *Angew. Chem., Int. Ed.*, 2012, **51**, 1437–1442.

103 A. Dawydow, R. Gueta, D. Ljaschenko, S. Ullrich, M. Hermann, N. Ehmann, S. Gao, A. Fiala, T. Langenhan, G. Nagel and R. J. Kittel, Channelrhodopsin-2–XXL, a powerful optogenetic tool for low-light applications, *Proc. Natl. Acad. Sci. U. S. A.*, 2014, **111**, 13972–13977.

104 E. Pastrana, Optogenetics: controlling cell function with light, *Nat. Methods*, 2010, **8**, 24–25.

105 T. Kim, M. Folcher, M. D. E. Baba and M. Fussenegger, A Synthetic erectile optogenetic stimulator enabling blue-light-inducible penile erection, *Angew. Chem., Int. Ed.*, 2015, **54**, 5933–5938.

106 A. H. All, X. Zeng, D. B. L. Teh, Z. Yi, A. Prasad, T. Ishizuka, N. Thakor, Y. Hiromu and X. Liu, Expanding the Toolbox of upconversion nanoparticles for *in vivo* optogenetics and neuromodulation, *Adv. Mater.*, 2019, 1803474.

107 A. Pliss, T. Y. Ohulchanskyy, G. Chen, J. Damasco, C. E. Bass and P. N. Prasad, Subcellular optogenetics enacted by targeted nanotransformers of near-infrared light, *ACS Photonics*, 2017, **4**, 806–814.

108 X. Lin, X. Chen, W. Zhang, T. Sun, P. Fang, Q. Liao, X. Chen, J. He, M. Liu, F. Wang and P. Shi, Core–shell–shell upconversion nanoparticles with enhanced emission for wireless optogenetic inhibition, *Nano Lett.*, 2018, **18**, 948–956.

109 T. Zhao, L. Chen, Q. Li and X. Li, Near-infrared light triggered drug release from mesoporous silica nanoparticles, *J. Mater. Chem. B*, 2018, **6**, 7112–7121.

110 E. Ruggiero, J. Hernández-Gil, J. C. Mareque-Rivas and L. Salassa, Near infrared activation of an anticancer PtIV complex by Tm-doped upconversion nanoparticles, *Chem. Commun.*, 2015, **51**, 2091–2094.

111 J. Shen, G. Chen, T. Y. Ohulchanskyy, S. J. Kesseli, S. Buchholz, Z. Li, P. N. Prasad and G. Han, Tunable near infrared to ultraviolet upconversion luminescence enhancement in (α-NaYF$_4$: Yb, Tm)/CaF$_2$ core/shell nanoparticles for In situ real-time recorded biocompatible photoactivation, *Small*, 2013, **9**, 3213–3217.

112 W. Zheng, P. Huang, Z. Gong, D. Tu, J. Xu, Q. Zou, R. Li, W. You, J.-C. G. Bünzli and X. Chen, Near-infrared-triggered photon upconversion tuning in all-inorganic cesium lead halide perovskite quantum dots, *Nat. Commun.*, 2018, **9**, 3462.

113 L. M. Jin, X. Chen, C. K. Siu, F. Wang and S. F. Yu, Enhancing multiphoton upconversion from NaYF$_4$:Yb/Tm@NaYF$_4$ core–shell nanoparticles via the use of laser cavity, *ACS Nano*, 2017, **11**, 843–849.

114 H. Zhu, A. Q. Chen, Y. Y. Wu, W. F. Zhang, S. C. Su, X. Ji, P. T. Jing, S. F. Yu, C. X. Shan and F. Huang, Seven-photon-excited upconversion lasing at room temperature, *Adv. Opt. Mater.*, 2018, **6**, 1800518.

115 C. Klusmann, J. Oppermann, P. Forster, C. Rockstuhl and H. Kalt, Identification of dielectric, plasmonic, and hybrid modes in metal-coated whispering-gallery-mode resonators, *ACS Photonics*, 2018, **5**, 2365–2373.

116 Y. Yao, J. Yao, V. K. Narasimhan, Z. Ruan, C. Xie, S. Fan and Y. Cui, Broadband light management using low-Q whispering gallery modes in spherical nanoshells, *Nat. Commun.*, 2012, **3**, 664.

117 Y. Zheng, Z. Fang, S. Liu, Y. Cheng and X. Chen, High-Q Exterior whispering-gallery modes in a double-layer crystalline microdisk resonator, *Phys. Rev. Lett.*, 2019, **122**, 253902.

118 Q. Zeng, E. Lafalce, C. H. Lin, M. J. Smith, J. Jung, Y. Yoon, Z. Lin, V. V. Tsukruk and Z. V. Vardeny, Control of whispering gallery modes and PT-symmetry breaking in colloidal quantum dot microdisk lasers with engineered notches, *Nano Lett.*, 2019, **19**, 6049–6057.

119 L. Jin, Y. Wu, Y. Wang, S. Liu, Y. Zhang, Z. Li, X. Chen, W. Zhang, S. Xiao and Q. Song, Mass-manufactural lanthanide-based ultraviolet B microlasers, *Adv. Mater.*, 2019, **31**, 1807079.

120 H. J. Bae, S. Bae, C. Park, S. Han, J. Kim, L. N. Kim, K. Kim, S. H. Song, W. Park and S. Kwon, Biomimetic microfingerprints for anti-counterfeiting strategies, *Adv. Mater.*, 2015, **27**, 2083–2089.

121 K. Jiang, L. Zhang, J. Lu, C. Xu, C. Cai and H. Lin, Triple-mode emission of carbon dots: applications for advanced anti-counterfeiting, *Angew. Chem., Int. Ed.*, 2016, **55**, 7231–7235.

122 B. Chen, W. Kong, Y. Liu, Y. Lu, M. Li, X. Qiao, X. Fan and F. Wang, Crystalline hollow microrods for site-selective enhancement of nonlinear photoluminescence, *Angew. Chem., Int. Ed.*, 2017, **56**, 10383–10387.

123 M. You, J. Zhong, Y. Hong, Z. Duan, M. Lin and F. Xu, Inkjet printing of upconversion nanoparticles for anti-counterfeit applications, *Nanoscale*, 2015, **7**, 4423–4431.

124 T. Sun, B. Xu, B. Chen, X. Chen, M. Li, P. Shi and F. Wang, Anti-counterfeiting patterns encrypted with multi-mode luminescent nanotaggants, *Nanoscale*, 2017, **9**, 2701–2705.

125 B. Chen, T. Sun, X. Qiao, X. Fan and F. Wang, Directional light Emission in a single $NaYF_4$ microcrystal via photon upconversion, *Adv. Opt. Mater.*, 2015, **3**, 1577–1581.

126 H. Zou, X. Yang, B. Chen, Y. Du, B. Ren, X. Sun, X. Qiao and F. Wang, Thermal Eenhancing of upconversion by negative lattice expansion in orthorhombic $Yb_2W_3O_{12}$, *Angew. Chem., Int. Ed.*, 2019, **58**, 17255–17259.

127 W. You, D. Tu, R. Li, W. Zheng and X. Chen, "Chameleon-like" optical behavior of lanthanide-doped fluoride nanoplates for multilevel anti-counterfeiting applications, *Nano Res.*, 2019, **12**, 1417–1422.